Commensurate-incommensurate phase transition in chlorine monolayer chemisorbed on Ag(111): Direct observation of crowdion condensation into a domain-wall fluid

Boris V. Andryushechkin, Vladimir Cherkez, Bertrand Kierren, Yannick Fagot-Revurat, Daniel Malterre, Konstantin N. Eltsov

Commensurate-incommensurate phase transition in chlorine monolayer chemisorbed on Ag(111): Direct observation of crowdion condensation into a domain-wall fluid

B. V. Andryushechkin,[1,*] V. V. Cherkez,[1,2] B. Kierren,[2] Y. Fagot-Revurat,[2] D. Malterre,[2] and K. N. Eltsov[1,3]

[1]*International Joint Laboratory IMTAS, A. M. Prokhorov General Physics Institute, Russian Academy of Sciences, Vavilov str. 38, RU-119991 Moscow, Russia*

[2]*International Joint Laboratory IMTAS, Institut Jean Lamour - UMR CNRS 7198 - équipe 102, Departement Physique de la Matière et des Matériaux, B.P 239 - Université H. Poincaré - Nancy, FR-54506 Vandoeuvre les Nancy, France*

[3]*Moscow Institute of Physics and Technology, Institutskii per. 9, RU-141700 Dolgoprudny, Moscow Region, Russia*

(Received 9 August 2011; revised manuscript received 26 October 2011; published 14 November 2011)

The commensurate-incommensurate phase transition in chlorine monolayer on Ag(111) has been studied with low-temperature scanning tunneling microscopy and low-energy electron diffraction. We report the observation of self-interstitial defects: two-dimensional (2D) crowdions formed at the initial stage of the $(\sqrt{3} \times \sqrt{3})$R30° lattice compression. After critical coverage of 0.34 monolayer (ML) the crowdions condense into a domain-wall fluid. As coverage further increases, the domain-wall crystal solidifies with average wall separation of 23 Å.

DOI: 10.1103/PhysRevB.84.205422 PACS number(s): 68.43.Fg, 68.43.Bc, 68.47.Fg, 68.55.ag

I. INTRODUCTION

In this paper, we consider Cl/Ag(111) system from the viewpoint of physics of two-dimensional phase transitions. Numerous theoretical papers were published in 1970–80s discussing the peculiarities of the commensurate-incommensurate (C-I) phase transitions in two dimensions (for reviews see Refs. 1–4). According to the theory, the C-I phase transition occurs via formation of the domain walls (DWs).[1] Evidence of domain-wall formation was supported by many diffraction experiments performed first for adsorption of noble gases on graphite[5–7] and on metals (see, for example, Ref. 8). Lately, domain walls were found in many other physisorbed and chemisorbed systems.

For adsorbate on triangular lattice, domain walls can be striped or hexagonal, depending of the sign of the crossing energy. If they are striped, the C-I phase transition is continuous; if they are hexagonal, there is a first-order phase transition.[9] By density of atoms, domain walls are classified as light, super light, heavy, and super heavy.[10]

The advent of scanning tunneling microscopy (STM) has opened a possibility of real-space investigations down to the atomic scale. Although scanning tunneling microscopy has been applied to the structural studies of physisorbed adsorbates since the 1990s,[11,12] the number of papers with new insights of the commensurate-incommensurate phase transitions is rather small.[13–15]

Halogens adsorbed on metal surfaces appear to be good model systems to study the commensurate-incommensurate phase transitions in two dimensions. Indeed, it has been demonstrated that for Cl/Cu(111),[16] I/Cu(111),[17] I/Au(111),[18] and I/Ag(111)[19] systems the compression of the commensurate $(\sqrt{3} \times \sqrt{3})$R30° lattice, generally formed by halogens on (111) planes of fcc metals, occurs via formation of the striped domain walls. The characteristic feature of all these systems is that six-spots triangles are observed around former $(\sqrt{3} \times \sqrt{3})$R30° spots positions in low energy electron diffraction (LEED). According to the classification done by Zeppenfeld *et al.*,[10] such a kind of splitting corresponds to the striped superheavy domain walls. Note also that in contrast to the case of physisorbed gases, the C-I phase transition in halogen layers can be investigated at room temperature with both STM and LEED.

In the work of Shard *et al.*,[20] similar triangles in LEED patterns were reported for the Cl/Ag(111) system but only at temperatures below 190 K. We believe that for this system, the commensurate-incommensurate phase transition also takes place via formation of striped domain walls. In order to look into the transition, we used a low-temperature STM operating at 5 K to obtain new data at the initial stage of the C-I transition, when the density of domain walls is low and diffraction techniques do not work. The aim of the paper was to follow step-by-step the phase transition from the early stages to the formation of the compressed lattice.

II. EXPERIMENTAL

All experiments were carried out in a multichamber UHV setup equipped with Omicron low temperature scanning tunneling microscope (LT-STM) (5–77 K) and LEED optics. Adsorption of molecular chlorine was done using a fine leak piezo valve. To prepare the Ag(111) sample ("Surface Preparation Laboratory"), repetitive cycles of Ar^+ sputtering (1 keV) and annealing (800 K) were used. The temperature of the sample during chlorine adsorption could be varied in the range 130–300 K.

III. RESULTS AND DISCUSSION

Figure 1 demonstrates a series of diffraction patterns recorded during step-by-step adsorption of Cl_2 onto Ag(111) surface at 300 K. The LEED pattern that develops initially is a so-called "diffused $(\sqrt{3} \times \sqrt{3})$R30°"[20–25] [see Fig. 1(b)]. The further dosing of chlorine gives rise to a "complex" pattern of numerous spots around the (3×3) positions[20–25] [see Figs. 1(c) and 1(d)]. In our recent studies,[26,27] we have demonstrated that such a pattern forms as a result of the diffraction on the system of small antiphase domains of the (3×3) reconstruction formed on Ag(111) surface at coverage close to the saturation.

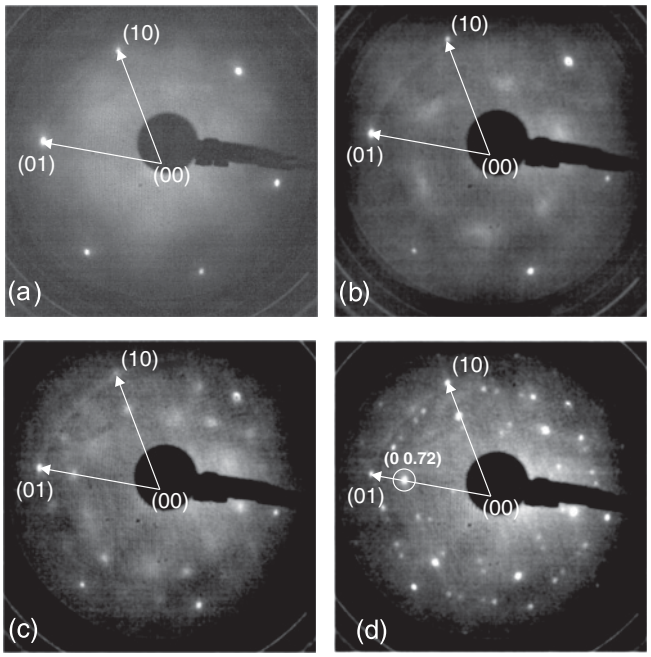

FIG. 1. Evolution of LEED pattern ($E_0 = 90$ eV) during continuous chlorine adsorption on Ag(111) surface at 300 K. The reciprocal lattice vectors of silver surface are shown. (a) Clean Ag (1×1), (b) "diffuse" Ag(111)-($\sqrt{3} \times \sqrt{3}$)R30° pattern, (c) development of "complex" [split (3×3)] pattern at coverage close to the saturation level, and (d) sharp "complex" [split (3×3)] pattern corresponding to the saturated layer of chlorine.

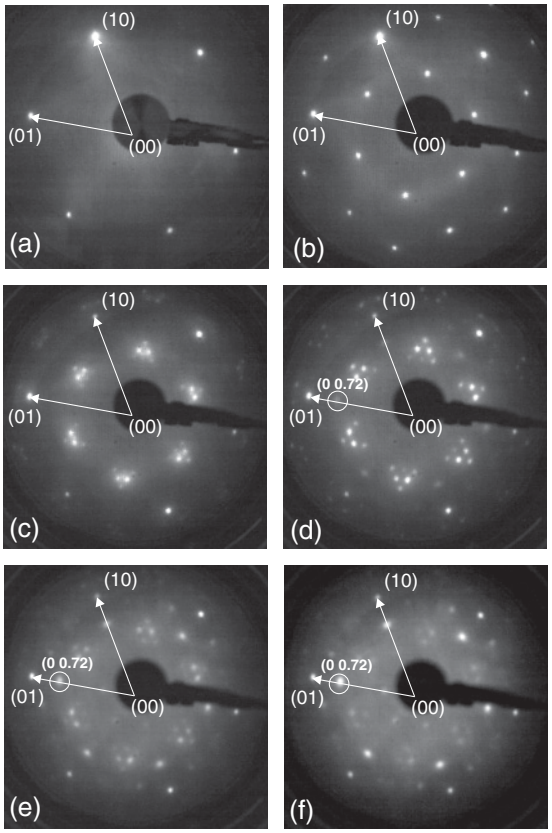

FIG. 2. Evolution of LEED pattern ($E_0 = 90$ eV) during continuous chlorine adsorption on Ag(111) surface at 130 K. The reciprocal lattice vectors of silver surface are shown. (a) Clean Ag (1×1), (b) sharp Ag(111)-($\sqrt{3} \times \sqrt{3}$)R30°, (c) "triangle" pattern, (d) and (e) coexistence of "triangle" and "complex" [split (3×3)] patterns, and (f) "complex" [split (3×3)] pattern corresponding to the saturated layer of chlorine.

In Fig. 2, we present the same series of LEED patterns, but obtained at 130 K. At the initial stage of adsorption, a sharp ($\sqrt{3} \times \sqrt{3}$)R30° pattern is observed [see Fig. 2(b)]. The increase of chlorine coverage resulted in the broadening and subsequent splitting of the $\sqrt{3}$ spots into six-spot triangles is in good correspondence with data by Shard *et al.*[20] [see Fig. 2(c)]. At some critical coverage [see Fig. 2(d)], new spots corresponding to 0.72 reciprocal lattice units of Ag(111) appeared in the diffraction pattern. Further dosing of Cl_2 resulted in a decrease of intensity of the six-spots triangles and development of the "complex" pattern corresponding to the (3 × 3) reconstruction [see Figs. 2(e) and 2(f)].

As the surface with a sharp ($\sqrt{3} \times \sqrt{3}$)R30° pattern is heated to room temperature, overlayer spots disappear, while doing the same to the system with six-spot triangles creates a "diffused ($\sqrt{3} \times \sqrt{3}$)R30°" pattern similar to the one shown in Fig. 1(b). Note that for both cases, these transitions are reversible.

Taking into account that ordering of the chlorine layer on Ag(111) takes place at low temperatures,[20] further chlorine adsorption was performed at 130 K. This allowed us to check the surface structure by LEED just before STM measurements.

Figure 3 presents an LT-STM image (5 K) of chlorinated surface corresponding to a sharp ($\sqrt{3} \times \sqrt{3}$)R30° LEED pattern. A clearly seen hexagonal lattice with a parameter of about 5 Å is naturally assigned to a simple commensurate ($\sqrt{3} \times \sqrt{3}$)R30° structure with one chlorine atom per unit mesh (exact coverage 0.33 monolayer (ML)). The black depressions in the STM image in Fig. 3 are assigned to Cl-atom vacancies. According to DFT calculations,[32] chlorine atoms prefer to occupy threefold hollow adsorption sites with a tiny difference in the adsorption energy between fcc and hcp sites. Since the interatomic distances in ($\sqrt{3} \times \sqrt{3}$)R30° lattice appear to be much larger than the van der Waals diameter of chlorine (3.6 Å), one may expect the compression of the chlorine lattice at a coverage above 0.33 ML. The mechanism of this compression is of fundamental importance.

Figure 4 presents an atomic-resolution STM image obtained for chlorine coverage of 0.34 ML. Although $\sqrt{3}$ spots in both the diffraction pattern and in the Fourier transformation image remain sharp, the real-space STM image changes dramatically, with numerous three-arm starlike objects parallel to the ⟨112⟩ directions. In the reciprocal space, the array of similar starlike objects gives rise to a specific diffuse hexagon seen in the insert to Fig. 4(a).

Figure 4(b) shows a magnified STM image of the star with a superimposed hexagonal grid corresponding to silver (1 × 1) lattice. The superimposition was made assuming that atoms around the star occupy threefold hollow sites. According to Fig. 4, the origin of the star is explained by the presence of an additional chlorine atom in the center. This atom can be considered to be a self-interstitial defect in the commensurate ($\sqrt{3} \times \sqrt{3}$)R30° lattice indicating the local compression of chlorine layer. The chlorine lattice remains commensurate with

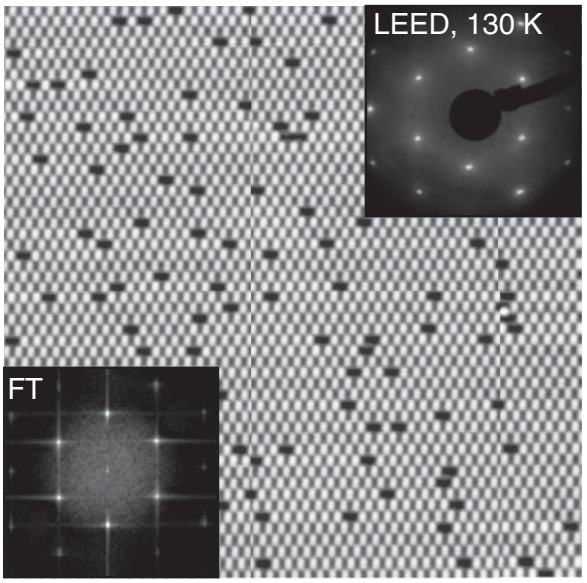

FIG. 3. STM image (250×250 Å^2, $I_t = 1$ nA, $U_s = -500$ mV, $T = 5$ K) of chlorine ($\sqrt{3} \times \sqrt{3}$)R30° structure formed at coverage $\theta \approx 0.32$ ML. Fourier transformation of the STM image and corresponding LEED pattern are shown in the left bottom and right upper corners, respectively.

a substrate and does not split into separate domains. The visual "star" effect in the STM images is explained by the narrowing of the interatomic distances in the directions of the stars' arms.

Thus we have found a new object assigned as a two-dimensional (2D) surface crowdion. Crowdions have been studied in bulk materials since the late 1950's.[28,29] Recently, formation of 1D surface crowdions has been suggested as a mechanism for surface adatom transport on strained Cu(100) and Pt(100) surfaces.[30,31] Here, we found a unique system to study 2D surface crowdions experimentally, in which surface crowdions were observed in real space.

The additional chlorine atom in the center of a crowdion in Fig. 4(b) occupying a threefold position similar to surrounding atoms, however, belongs to another ($\sqrt{3} \times \sqrt{3}$)R30° sublattice (marked as "2" in Fig. 5). There are three equivalent ($\sqrt{3} \times \sqrt{3}$)R30° sublattices on the (111) surface of fcc metals. Therefore another type of crowdion should exist, with a central atom belonging to sublattice "3." Models of both types of crowdions exhibiting a different chirality are shown in Fig. 5. The size of the crowdions could be estimated by the perturbation of atom positions caused by the interstitial atom. As follows from Fig. 4(b), the perturbation attenuates at three to four interatomic distances, which corresponds to the crowdion diameter, about 30 Å.

At further increase of the chlorine coverage ($\theta > 0.34$ ML), $\sqrt{3}$ spots split into six-spots triangles in LEED [see Figs. 2(c) and 2(d)]. The corresponding STM image in Fig. 6(a) exhibits not only the atomic modulation, but also a striped superstructure with a period about 23 Å. Three possible orientations of the stripes apparently seen in the STM image coincide with the base directions of the close-packed atomic rows in a ($\sqrt{3} \times \sqrt{3}$)R30° lattice. The interatomic distances measured along the stripes are in a good agreement with nearest-neighbor distances in a ($\sqrt{3} \times \sqrt{3}$)R30° lattice (5 Å), while average

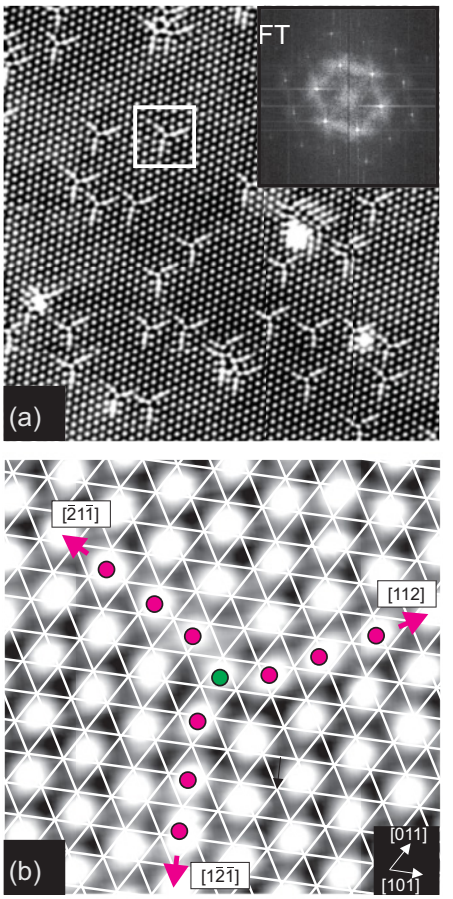

FIG. 4. (Color online) (a) STM image (330×330 Å^2, $I_t = 2.8$ nA, $U_s = -60$ mV, $T = 5$ K) of Ag(111) surface covered with $\theta \approx 0.34$ ML of chlorine. In the upper right corner, FT of the STM image is shown. (b) Zoom from image (a) superimposed with a grid, the knots of the grid coincide with position of substrate atoms. A self-interstitial defect (additional Cl atom) in the ($\sqrt{3} \times \sqrt{3}$)R30°-Cl structure is highlighted with a green circle and the distorted chlorine atoms incommensurate structure with purple circles.

distances along the other two close-packed atomic rows appear to be lower. This clearly shows that the compression of the chlorine lattice is uniaxial. The visible modulation arises due to variation of density of atomic rows in the direction of compression and due to the modulation of the adsorption height of chlorine atoms in different adsorption sites. More closely packed rows are visualized as bright areas, while areas with lower density are visualized as darker ones. The interatomic distances in the dark stripes (5 Å) are the same as in the ($\sqrt{3} \times \sqrt{3}$)R30° structure, while in the bright stripes they are lower (4.2 Å). We believe that the striped structure in Fig. 6(a) reflects the formation of regular-spaced striped domain walls separating the ($\sqrt{3} \times \sqrt{3}$)R30° domains. We assign the bright areas to the domain walls. The Fourier transform of the STM image shown in Fig. 6(b) contains characteristic six-spots triangles similar to those observed in LEED. The FT-STM image for the single domain shown in the insert to Fig. 6(a) demonstrates splitting in the direction perpendicular to the stripes, indicating the uniaxial compression of the chlorine layer. The observation of the six-spots triangles both in FT

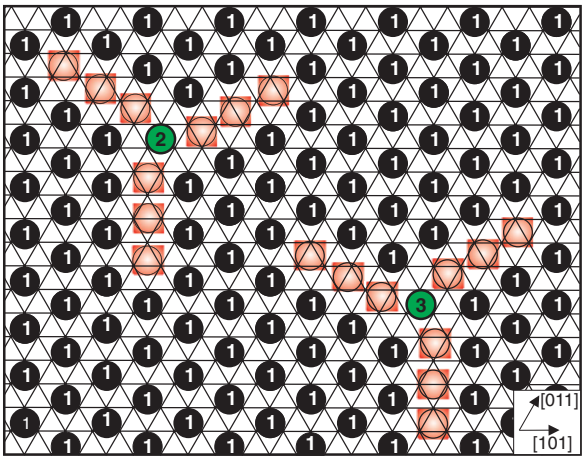

FIG. 5. (Color online) A schematic representation of two types of crowdions (with left- and right-side chirality) in the $(\sqrt{3} \times \sqrt{3})$R30°-Cl structure. Chlorine atoms in different $(\sqrt{3} \times \sqrt{3})$R30° sublattices are marked with numbers 1, 2, and 3. Disturbed chlorine atoms forming crowdions are shown in pink. Additional chlorine atoms in the centers of crowdions (interstitials) are shown in green.

and LEED is a result of the combination of contributions from areas with three different directions of compression rotated by 120°, as shown in Fig. 6(c).

To describe the structure in detail, we superimposed the atomic-resolution STM image with an atomic grid of the substrate [see Fig. 7(a)]. The superimposition was based

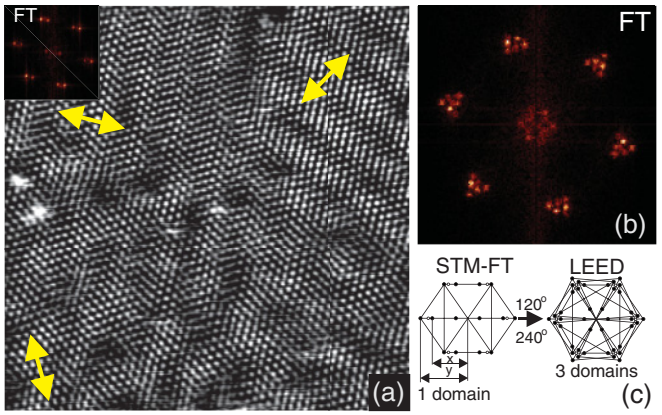

FIG. 6. (Color online) (a) STM image (250×250 Å^2, $I_t = 0.25$ nA, $U_s = -1$ V, $T = 5$ K) of chlorine layer on Ag(111). Three domains with different direction of the stripes are clearly seen. The insert shows Fourier Transform (FT) for the one domain. (b)Fourier Transform of the STM image from (a). (c) The model drawing demonstrating formation of triangles in LEED and FT-STM patterns. The FT-STM patterns corresponding to three possible orientations (0, 120, and 240 degrees) of the uniaxial compressed layer are shown on the left. Spot positions were marked by filled circles. Open circles indicate the positions of the spots in the $(\sqrt{3} \times \sqrt{3})$R30° structure. The scheme on the right is constructed as a superposition of patterns shown on the left and, hence, takes into account three possible directions of compression. Due to a low lateral resolution of the LEED technique, a diffraction pattern always contains contribution from areas with different direction of compression and corresponds to the scheme on the right.

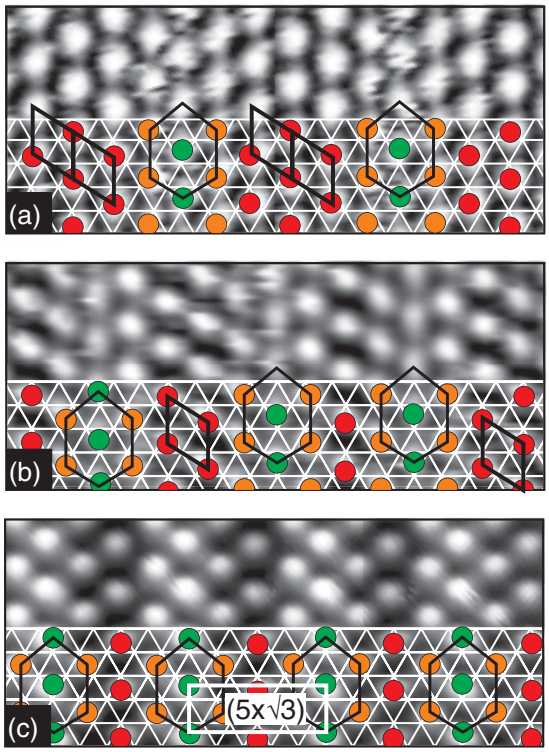

FIG. 7. (Color online) STM images (57×24 Å^2, $T = 5$ K) for different domain-wall distances. (a) $l = 8a$, (b) $l = 6.5a$ and $l = 5a$, and (c) $l = 5a$. Red balls indicate atoms in threefold positions belonging to $(\sqrt{3} \times \sqrt{3})$R30° domains. Green and orange balls form domain walls. Green balls show atoms in threefold positions (different from red). Orange balls correspond to atoms in bridge positions.

on the assumption that the interatomic distances along the stripes are equal to the ones in the $(\sqrt{3} \times \sqrt{3})$R30° lattice. Chlorine atoms in the center of the domains were placed in threefold positions assuming that their adsorption sites should be the same as in the $(\sqrt{3} \times \sqrt{3})$R30° lattice. We do not try to assume whether the adsorption sites of atoms in the $(\sqrt{3} \times \sqrt{3})$R30° lattice are fcc or hcp because the difference in adsorption energy is too small.[32] The neighboring domains were found to be antiphase to each other with the phase shift characteristic to the striped superheavy domain walls. According to our experimental data, relaxation of domain walls was detected. A domain wall in the present case consists of three atomic rows, with interrow distances lower than in the $(\sqrt{3} \times \sqrt{3})$R30° lattice. Atoms forming the central row of the domain wall occupy threefold positions [other than in the $(\sqrt{3} \times \sqrt{3})$R30° domain], while the atoms in the two neighboring rows occupy positions close to bridge. The lowest interatomic distance derived from the STM images was determined to be 4.2 Å. The distance between DWs in Fig. 7(a) is equal to $8a = 23.1$ Å [a is an Ag(111) lattice constant].

According to LEED data from Fig. 2, the size of the six-spots triangles is growing in parallel with the development of the spots belonging to the "complex" LEED pattern. Increase of the splitting means the contraction of the domain-wall distance.[10] The domain-wall distance for the striped super-heavy domain walls is determined by the equation $l = a(2 + 1.5n)$ $(n = 1,2,3\ldots)$.[15,33] In Fig. 7(b), we present

a fragment of the STM images for a more compressed phase corresponding to a combination of shorter domain-wall distances: 18.8 Å (6.5a, $n = 3$) and 14.5 Å (5a, $n = 2$). In Fig. 7(c), the STM image of the maximum compressed phase with $l = 14.5$ Å (5a, $n = 2$) is presented. A simple analysis of the STM image from Fig. 7(b) shows that for $l = 6.5a$, one can draw only one $(\sqrt{3} \times \sqrt{3})$R30° unit cell between the walls. For $l = 5a$, the $(\sqrt{3} \times \sqrt{3})$R30° domains degenerate into one atomic row, as is evident from Fig. 7(c). Moreover, the structure in Fig. 7(c) can already be considered to be a high-order commensurate structure $(5\times\sqrt{3})$.

The splitting in LEED and FT-STM patterns can be described by the x/y ratio [see model drawing in Fig. 6(c)], which is equal to $(n + 1)/(n + 2)$.[17] The experimental value of the splitting parameter x/y determined for STM images from Fig. 6 was found to be 0.83 ± 0.01. It corresponds with a high accuracy to $n = 4$ and a domain-wall distance of $8a = 23.1$ Å. This value coincides with the distance measured directly from STM in Fig. 7(a). In the frame of the striped superheavy DWs, the domain-wall distance l and the coverage θ are coupled by $l = a/(3\theta - 1)$.[15,33] In these terms, chlorine coverage can be accurately calculated: $\theta_{8a} = 0.375$ ML.

The x/y ratio corresponding to the maximum size of the six-spots triangles measured from the experimental LEED patterns is equal to 0.76 ± 0.01. This value can be perfectly reproduced by the domain-wall network with $n = 2$ and $l = 5a$ (14.5 Å) formed at the local coverage of $\theta_{5a} = 0.40$ ML. In other words, the uniaxial compression of chlorine layer ends on the $(5\times\sqrt{3})$ structure shown in Fig. 7(c).

At the intermediate coverage range $\theta < 0.37$ ML, both crowdions and domain walls coexist on the surface, as shown in Fig. 8(a). We have found out that at certain scanning parameters ($I_t = 2$ nA, $U_s \approx +2$ V), the contrast is such that crowdions and domain walls become visible in STM images as dark spots and lines, respectively [see Fig. 8(b)]. This finding makes it possible to follow the C-I phase transition at a larger scale with higher scanning speed.

Figure 9 shows a series of 1000×1000 Å^2 STM images corresponding to the gradual increase of the coverage from 0.34 to 0.40 ML. To prepare areas with different coverages, we used the temperature dependence of the chlorine sticking probability on a silver surface.[23] The sample was cooled down to 130 K by attaching a cold finger on one side of the sample holder, thus creating a tiny temperature gradient across the sample. Accordingly, subsequent adsorption of chlorine created a coverage gradient. Therefore, to acquire the STM images shown in Fig. 9, we simply moved the STM tip across the sample.

Now we can follow the phase transition. At the first step of $(\sqrt{3} \times \sqrt{3})$R30° compression, only crowdions exist on the surface. Such a situation is shown in Fig. 9(a) and corresponds to a coverage of 0.34 ML (this coverage can be obtained directly from the STM image simply by counting the number of crowdions). At some critical density of crowdions (approximately corresponding to the average nearest-neighbor distances, about 20 Å), new objects, loop lines (domain walls), appeared. The increase of the coverage resulted in an increase of the length of the domain-wall loops. As the coverage increases, the density of domain walls grows, while the total number of crowdions decreases. According to Figs. 9(b) and 9(c), the domain-wall-to-crowdion, crowdion-to-crowdion, and domain-wall-to-domain-wall interactions are repulsive. For all three pairs of objects, the separations between them appear to be very close to ≈20 Å. In Fig. 9(c), the total length of the domain walls is large enough, but the ordering of domain walls just starts at this coverage. Ordering of domain walls starts in the areas where all crowdions disappear. The distances between parallel domain walls also appear to be equal to 20–25 Å. At coverage 0.37 ML (estimated by the period of the domain-wall lattice), almost all crowdions disappear and large areas with parallel striped domain walls can be seen in the STM image, as in Fig. 9(d).

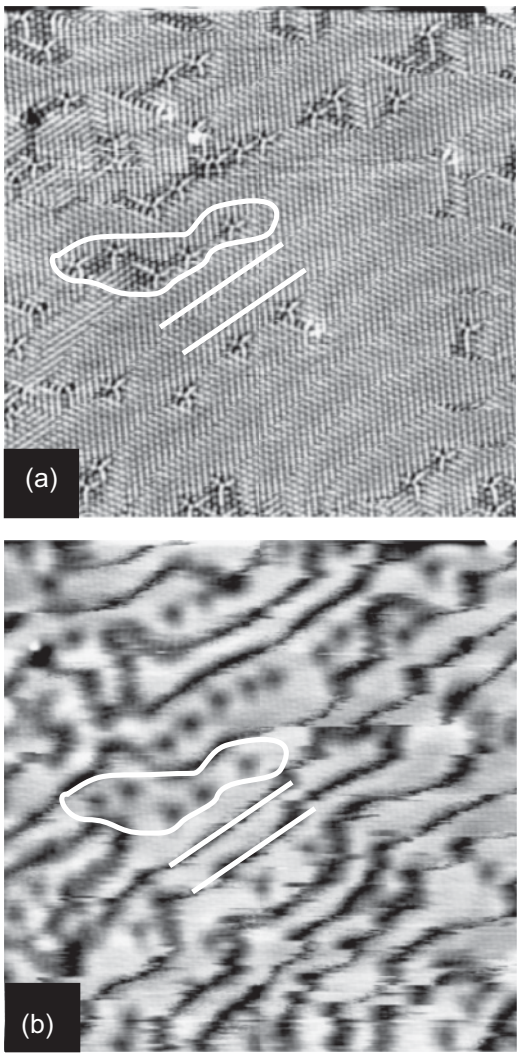

FIG. 8. STM images (330×330 Å^2, $T = 5$ K) of the same area of Ag(111) surface covered with chlorine. The image (a) was taken with usual scanning parameters $I_t = 2.9$ nA and $U_s = 48$ mV, whereas image (b) was taken with elevated bias voltage: $I_t = 2.9$ nA and $U_s = +1980$ mV. Additional contrast in the areas of increased chlorine density can be clearly seen on the image (b): crowdions appear as dark spots and domain walls as dark lines.

At $\theta > 0.38$ ML [see Fig. 9(d)], the STM image shows the formation of triangular islands of the 3×3 reconstruction described in detail in our previous work.[26] The 3×3 islands destroy the regular domain wall lattice. Indeed, now domain-

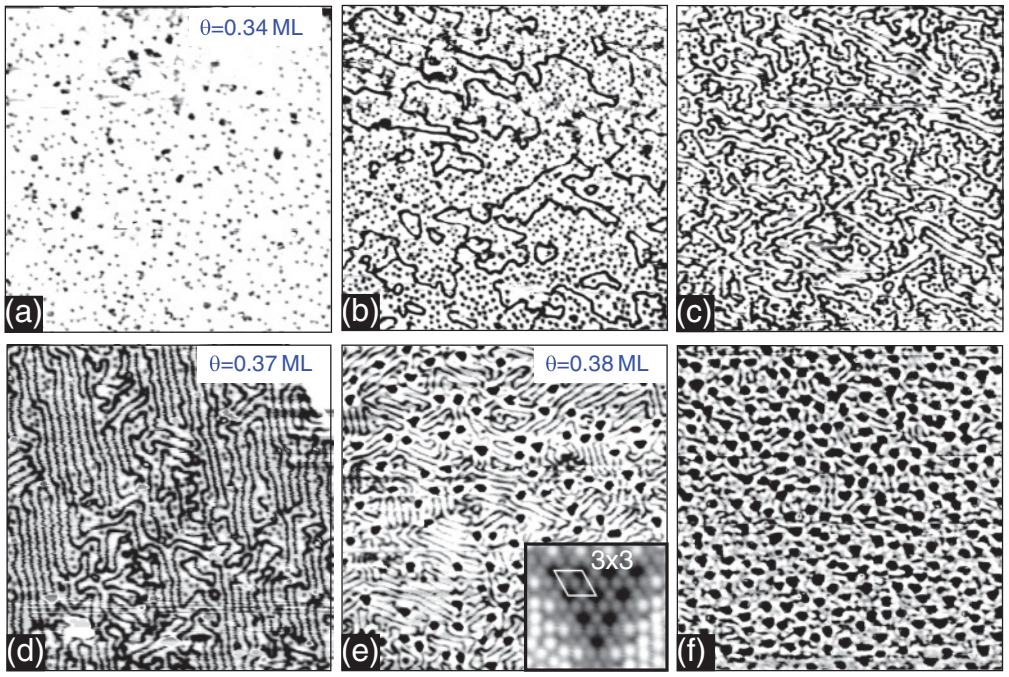

FIG. 9. (Color online) Large-scale STM images (1000×1000 Å^2, $I_t = 2.9$ nA, $U_s = +1980$ mV, $T = 5$ K) of Ag(111) surface during continuous increase of surface coverage in the range $0.34 < \theta < 0.40$ ML. (a) 2D gas of crowdions, (b) and (c) condensation of the crowdion gas into domain walls, (d) striped domain-wall structure (domain-wall crystal) formed at $\theta \approx 0.37$ ML, (e) and (f) nucleation and growth of the new (3×3) phase (small dark triangles) in parallel with continuous decrease of the domain-wall distance. The atomic-resolution STM image of the (3×3) island is shown in the insert to (e).

wall lines prefer to end at the 3×3 islands, as seen from Fig. 9(e). As coverage increases further, the domain-wall lattice breaks up into separate segments between areas with the 3×3 reconstruction [see Fig. 9(f)]. Finally, the domain-wall system degenerates into a compressed quasihexagonal lattice. At the saturation, unreconstructed areas disappear, leaving on the surface two phases: the islands with a (3×3) reconstruction and clusters Ag_3Cl_7.[26,27]

Thus we have shown that a 2D gas of crowdions condensates into domain walls. Since at the beginning of transition the domain walls are not ordered, they can be treated as a domain-wall fluid. An increase in the number of atoms on the surface leads to the solidification of the DW fluid and formation of an equally spaced DW lattice (DW crystal). Understanding the microscopic mechanism of the crowdion-to-domain-wall transition is of great scientific interest.

In Fig. 10, we show an STM image of an interesting object formed as a result of the agglomeration of crowdions (marked as "1"). The superimposition of the atomic grid of the substrate shows that the core of the object contains three chlorine atoms with a nearest-neighbor distance of 5 Å [the distance in a $(\sqrt{3} \times \sqrt{3})$R30° lattice] occupying threefold hollow sites. However, atoms in the core belong to another $(\sqrt{3} \times \sqrt{3})$R30° sublattice than the surrounding chlorine atoms. In this connection, we interpret such a kind of object as a nucleus of the new domain belonging to a different $\sqrt{3}$ sublattice that is surrounded by the domain-wall loop. Atoms from the "arms" of the object occupying nonsymmetrical positions form segments of domain walls. As the additional chlorine atoms adsorb, the size of the core domain increases.

The STM image in Fig. 10 shows another object with linear geometry (marked as "2") formed near a surface defect. We consider this object to be formed by several crowdions. In fact, the "arms" in this case form a segment of a domain wall.

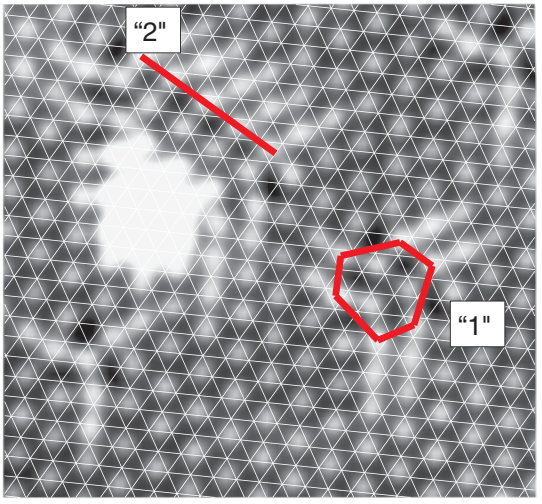

FIG. 10. (Color online) (STM images (66×62 Å^2, $I_t = 2.8$ nA, $U_s = -60$ mV, $T = 5$ K) showing the process of crowdions condensation. An object "1" is considered to be a nucleus of the domain-wall loop. Three atoms in the core of the object 1 formed a small domain out of phase with the surrounding chlorine lattice. A linear object "2" formed by several crowdions is assigned to the small segment of the growing domain wall. For clarity, domain walls are shown by red lines.

In their theoretical study, Lyuksyutov *et al.*[34] have shown that a 2D gas of the interstitial defects significantly influences the C-I phase transition. In particular, they considered the possibility of atom exchange between a 2D gas of the interstitials and domain walls. According to Ref. 34, heating of the domain-wall system leads to an incommensurate-commensurate phase transition via domain-wall evaporation. As a result, all excess of atoms (N) can be transferred to the gas of self-interstitials and domain walls disappear. Another consequence of the theory by Lyuksyutov *et al.*[34] concerns the stability of the domain-wall lattices at low N. The authors have shown that at $N \rightarrow 0$, the domain walls are thermodynamically unfavorable in comparison with a gas of pointlike defects. Such a conclusion is in excellent agreement with our data. Indeed, we detected that first DW lines appear at coverage $\theta >$ 0.34 ML.

An older theory by Vilain[35] predicts that at elevated temperatures, the striped DW structure with a large period is always unstable against a first-order transition to a hexagonal DW lattice. Lyuksyutov *et al.*[34] have shown that at $N \rightarrow 0$, the phase with pointlike defects is always thermodynamically preferred over a hexagonal DW lattice. Such conclusion is also in line with our experimental data, since the hexagonal DWs have been never detected in our STM images.

It is worth noting that in the experiment, we observe phase separation between crowdions and domain walls corresponding to a temperature of 5 K. At elevated temperatures, according to Lyuksyutov *at al.*,[34] the condensation of crowdions should occur at higher coverages.

IV. CONCLUSIONS

Thus we report a LEED-STM study of the commensurate-incommensurate phase transition in a chlorine monolayer on Ag(111). We have shown that the six-spots triangles in a LEED pattern observed by Shard *et al.*[20] at temperatures below 190 K correspond to the formation of an ordered array of striped superheavy domain walls ($0.375 < \theta <$ 0.40 ML). We explain the transformation of the six-spot triangles into diffuse spots at 300 K by the growth of DW fluctuations and by the formation of the fluid phase, an effect predicted by theoretical works.[1] This removes the uncertainty about the coverage corresponding to the "diffused" $(\sqrt{3} \times \sqrt{3})$R30° pattern observed by many authors in LEED at 300 K.[20–25]

We would like to emphasize that our study is an early attempt to investigate the initial stage of the C-I phase transition at the atomic level in real space. A huge collection of the available experimental data previously accumulated by many authors had been obtained using different diffraction techniques. As a result, such effects as the formation of the 2D gas of the interstitials and subsequent condensation into a DW fluid could hardly be imagined from diffraction data. Existing LT-STM data for the structure of noble gas films correspond to ordered DW lattices.[12–14] It is likely that monolayer films of the physisorbed gases are very soft at 5 K in comparison with a strongly chemisorbed chlorine monolayer. Indeed, we failed to observe crowdions at 55 K, although an ordered domain-wall lattice was easily imaged with an STM. We believe that at 55-K crowdions became too mobile to make imaging possible. For physisorbed gases even at 5 K, the movement of crowdions (that should probably exist) can make it difficult to investigate the initial stages of C-I phase transitions.

ACKNOWLEDGMENTS

The authors would like to thank G. M. Zhidomirov and O. M. Braun for fruitful discussions. This work was supported in part by grants of the Russian Foundation for Basic Research No. 10-02-90476-Ukr-a and by Contracts Nos. P2452, P2293, and P849 with Ministry of Education and Science of the Russian Federation.

*andrush@kapella.gpi.ru

[1] I. Lyuksyutov, A. G. Naumovets, and V. L. Pokrovsky, *Two-dimensional Crystals* (Academic, Boston, 1992).
[2] P. Bak, Rep. Prog. Phys. **45**, 587 (1982).
[3] B. N. J. Persson, Surf. Sci. Rep. **15**, 1 (1992).
[4] A. Patrykiejew, S. Sokolowski, and K. Binder, Surf. Sci. Rep. **37**, 209 (2000).
[5] M. den Nijs, *Phase Transitions and Critical Phenomena*, edited by C. Domb and J. L. Lebowitz (Academic, New York, 1988), Vol. 12, p. 219.
[6] H. Freimuth, H. Wiechert, H. P. Schildberg, and H. J. Lauter, Phys. Rev. B **42**, 587 (1990) and references therein.
[7] J. Cui and S. C. Fain, Phys. Rev. B **39**, 8628 (1989).
[8] K. Kern and G. Comsa, in *Chemistry and Physics of Solid Surfaces* VII, edited by R. Vanselow and R. Howe, Springer Series in Surface Sciences Vol. 10 (Springer, Heidelberg, 1988), p. 65.
[9] P. Bak, D. Mukamel, J. Villain, and K. Wentowska, Phys. Rev. B **19**, 1610 (1979).
[10] P. Zeppenfeld, K. Kern, R. David, and G. Comsa, Phys. Rev. B **38**, 3918 (1988).
[11] D. M. Eigler, P. S. Weiss, E. K. Schweizer, and N. D. Lang, Phys. Rev. Lett. **66**, 1189 (1991).
[12] S. Horch, P. Zeppenfeld, and G. Comsa, Appl. Phys. A **60**, 147 (1995).
[13] B. Grimm, H. Hövel, M. Pollmann, and B. Reihl, Phys. Rev. Lett. **83**, 991 (1999).
[14] F. Brunet, R. Schaub, S. Fédrigo, R. Monot, J. Buttet, and W. Harbich, Surf. Sci. **512**, 201 (2002).
[15] T. Müller, D. Heuer, H. Pfnür, and U. Köhler, Surf. Sci. **347**, 80 (1996).
[16] B. V. Andryushechkin, K. N. Eltsov, and V. M. Shevlyuga, Surf. Sci. **470**, L63 (2000).
[17] B. V. Andryushechkin, K. N. Eltsov, and V. M. Shevlyuga, Surf. Sci. **472**, 80 (2001).
[18] L. Huang, P. Zeppenfeld, S. Horch, and G. Comsa, J. Chem. Phys. **107**, 585 (1997).
[19] B. V. Andryushechkin, K. N. Eltsov, and V. V. Cherkez (unpublished).
[20] A. G. Shard and V. R. Dhanak, J. Phys. Chem. B **104**, 2743 (2000).

[21]G. Rovida, F. Pratesi, M. Maglietta, and E. Ferroni, Japan J. Appl. Phys. Suppl. **2**, 117 (1974).
[22]G. Rovida and F. Pratesi, Surf. Sci. **51**, 270 (1975).
[23]M. Bowker and K. C. Waugh, Surf. Sci. **134**, 639 (1983).
[24]P. J. Goddard and R. M. Lambert, Surf. Sci. **67**, 180 (1977).
[25]G. M. Lamble, R. S. Brooks, S. Ferrer, D. A. King, and D. Norman, Phys. Rev. B **34**, 2975 (1986).
[26]B. V. Andryushechkin, V. V. Cherkez, E. V. Gladchenko, G. M. Zhidomirov, B. Kierren, Y. Fagot-Revurat, D. Malterre, and K. N. Eltsov, Phys. Rev. B **81**, 205434 (2010).
[27]B. V. Andryushechkin, V. V. Cherkez, E. V. Gladchenko, G. M. Zhidomirov, B. Kierren, Y. Fagot-Revurat, D. Malterre, and K. N. Eltsov, Phys. Rev. B **84**, 075452 (2011).
[28]L. Tewordt, Phys. Rev. **109**, 61 (1958).
[29]O. M. Braun and Yu. S. Kivshar, *The Frenkel-Kontorova Model: Concepts, Methods, and Applications* (Springer-Verlag, Berlin, 2004).
[30]W. Xiao, P. A. Greaney, and D. C. Chrzan, Phys. Rev. Lett. **90**, 156102 (2003).
[31]W. Xiao, P. A. Greaney, and D. C. Chrzan, Phys. Rev. B **70**, 033402 (2004).
[32]N. H. de Leeuw, C. J. Nelson, C. R. A. Catlow, P. Sautet, and W. Dong, Phys. Rev. B **69**, 045419 (2004).
[33]R. Dennert, M. Sokolowski, and H. Pfnür, Surf. Sci. **271**, 1 (1992).
[34]I. F. Lyuksyutov, H. Pfnür, and H.-U. Everts, Europhys. Lett. **33**, 673 (1996).
[35]J. Villain, Surf. Sci. **97**, 219 (1980).